Resistance to miltefosine results from amplification of the *RTA3* floppase or inactivation of flippases in *Candida parapsilosis*

Sean A. Bergin[1*], Fang Zhao[1*], Adam P. Ryan[1], Carolin A. Müller[2], Conrad A. Nieduszynski[3], Bing Zhai[4,5,6], Thierry Rolling[4,5], Tobias M. Hohl[4,5,7], Florent Morio[8,9], Jillian Scully[1], Kenneth H. Wolfe[10] and Geraldine Butler[1].

* Equal contribution

[1] School of Biomolecular and Biomedical Science, Conway Institute, University College Dublin, Belfield, Dublin 4, Ireland
[2] Sir William Dunn School of Pathology, University of Oxford, Oxford, UK
[3] Earlham Institute, Norwich Research Park, Norwich NR4 7UZ, UK
[4] Infectious Disease Service, Department of Medicine, Memorial Sloan Kettering Cancer Center, New York, NY, USA
[5] Immunology Program, Sloan Kettering Institute, Memorial Sloan Kettering Cancer Center, New York, NY, USA
[6] Laboratory of Quantitative Engineering Biology, Shenzhen Institute of Synthetic Biology, Shenzhen Institutes of Advanced Technology, Chinese Academy of Sciences, Shenzhen, China
[7] Department of Medicine, Weill Cornell Medical College, New York, NY, USA
[8] Laboratoire de Parasitologie et Mycologie, CHU de Nantes, Nantes, France
[9] Cibles et Médicaments des Infections et du Cancer, IICiMed UPRES EA 1155, UFR de Sciences Pharmaceutiques et Biologiques, 1 rue Gaston Veil, 44035 Nantes, France
[10] School of Medicine, Conway Institute, University College Dublin, Belfield, Dublin 4, Ireland.

Running title: Miltefosine resistance in *Candida parapsilosis*

corresponding author: Geraldine Butler, School of Biomolecular and Biomedical Science, Conway Institute, University College Dublin, Belfield, Dublin 4, Ireland

email: gbutler@ucd.ie

Abstract

Flippases and floppases are two classes of proteins that have opposing functions in the maintenance of lipid asymmetry of the plasma membrane. Flippases translocate lipids from the exoplasmic leaflet to the cytosolic leaflet, and floppases act in the opposite direction. Phosphatidylcholine (PC) is a major component of the eukaryotic plasma membrane and is asymmetrically distributed, being more abundant in the exoplasmic leaflet. Here we show that gene amplification of a putative PC floppase or double disruption of two PC flippases in the pathogenic yeast *Candida parapsilosis* results in resistance to miltefosine, an alkylphosphocholine drug that affects PC metabolism that has recently been granted orphan drug designation approval by the US FDA for treatment of invasive candidiasis. We analysed the genomes of 170 *C. parapsilosis* isolates and found that 107 of them have copy number variations (CNVs) at the *RTA3* gene. *RTA3* encodes a putative PC floppase whose deletion is known to increase the inward translocation of PC in *Candida albicans*. *RTA3* copy number ranges from 2 to >40 across the *C. parapsilosis* isolates. Interestingly, 16 distinct CNVs with unique endpoints were identified, and phylogenetic analysis shows that almost all of them have originated only once. We found that increased copy number of *RTA3* correlates with miltefosine resistance. Additionally, we conducted an adaptive laboratory evolution experiment in which two *C. parapsilosis* isolates were cultured in increasing concentrations of miltefosine over 26 days. Two genes, *CPAR2_303950* and *CPAR2_102700*, gained homozygous protein-disrupting mutations in the evolved strains and code for putative PC flippases homologous to *S. cerevisiae DNF1.* Our results indicate that alteration of lipid asymmetry across the plasma membrane is a key mechanism of miltefosine resistance. We also find that *C. parapsilosis* is likely to gain resistance to miltefosine rapidly, because many isolates carry loss-of-function alleles in one of the flippase genes.

Author summary

Miltefosine was developed as an anticancer drug but is commonly used to treat infections with the protozoan parasites *Leishmania* and *Trypanosoma cruzi*. More recently, it has been used to treat fungal infections, and in 2021 it was designated as an orphan drug by the US Food and Drug Administration for treatment of invasive candidiasis. Miltefosine is a derivative of phosphatidylcholine (PC), a major constituent of the cell membrane. PC and other phospholipids are asymmetrically distributed across the cell membrane. The mechanism of action of miltefosine is unknown. Here, we show that either increasing the activity of a putative floppase, which controls outward “flop” movement of phospholipids, or decreasing the activity of flippases, which control inward “flip” movement, results in

increased resistance of the fungal pathogen *Candida parapsilosis* to miltefosine. This result suggests that miltefosine acts by controlling the localisation of PC or other phospholipids in the membrane. Importantly, we find that many *C. parapsilosis* isolates carry mutations in one flippase gene, which renders them partially resistant to miltefosine, and prone to easily acquiring increased resistance.

Introduction

Lipids in yeast plasma membranes belong to three main families: sterols, sphingolipids, and phospholipids (or glycerophospholipids) [1]. Phospholipids (including phosphatidylcholine (PC), phosphatidylethanolamine (PE), phosphatidylinositol (PI), and phosphatidylserine (PS)) and sphingolipids (including the long chain bases (LCBs) dihydrosphingosine (DHS) and phytosphingosine (PHS)) are distributed asymmetrically in the plasma membrane bilayer [2, 3]. Plasma asymmetry is determined by the action of lipid translocators via rapid inward (flip) and outward (flop) movements [4]. Most flippases are members of the P4-ATPase family [5], and most floppases are ABC-type transporters [6]. The Rta1 family of 7 transmembrane domain proteins are also predicted lipid transporters [7].

Several antimicrobial drugs are targeted against lipid synthesis, such as azole drugs, which target ergosterol synthesis in fungi [8-10]. Miltefosine (hexadecylphosphocholine) is an alkylphosphocholine derivative that inhibits PC biosynthesis or localization [11]. Miltefosine was initially investigated as an antitumor agent, but it was found to have a very limited anticancer effect [12]. However, it has been used successfully to treat infections with *Leishmania* and *Trypanosoma cruzi* [13-15]. Recently, miltefosine has also been shown to have antifungal activity, including against *Aspergillus* [16], *Cryptococcus* [17] and *Paracoccidioides* [18]. Anti-*Candida* activity has also been reported, including against *Candida auris* [19, 20], *Candida krusei* [21] and *Candida albicans*, where it inhibits growth of both planktonic and biofilm cells [22]. In 2021, miltefosine was granted orphan drug designation approval by the US Food and Drug Administration (FDA) for treatment of invasive candidiasis (https://www.accessdata.fda.gov/scripts/opdlisting/oopd/detailedIndex.cfm?cfgridkey=843921).

The mechanism of action of miltefosine is not completely understood. In liver cells, miltefosine is proposed to reduce the biosynthesis of PC by inhibiting the activity of CTP:phosphocholine cytidylyltransferase (CT) and PE N-methyltransferase activity [23]. Treatment of *Leishmania* with miltefosine decreases the amount of PC and increases PE in the membrane, because of a reduction of intracellular choline [24]. In addition, cytochrome c activity in the mitochondria is inhibited, and the plasma membrane Ca^{2+} channel is disrupted [25]. Studies in *Saccharomyces cerevisiae* suggest that related drugs, such as edelfosine (lysophosphatidylcholine) also disrupt lipid rafts in the cell membrane, perhaps by directly interacting with sterols [26]. In *Aspergillus fumigatus*, miltefosine affects metabolism of lipids and fatty acids, as well as by increasing mitochondrial fragmentation [16].

Most flippases belonging to the P4-ATPase family, which consist of two subunits, a catalytic alpha-subunit with 10 transmembrane alpha-helices, and a beta-subunit with two transmembrane alpha-helices belonging to the Cdc50 family [5]. Flipping of PE, PS and PC is specifically associated with Class 3 P4-ATPases, represented by Dnf1 and Dnf2 in *S. cerevisiae* [27]. Disruption of *DNF1* or *DNF2*, or of *LEM3* (*CDC50*), results in miltefosine resistance in *S. cerevisiae* [28]. Similarly, mutations in P4-ATPases in *Leishmania* species confer resistance to miltefosine [29-32].

In *Candida* species, flippases have not yet been associated with miltefosine resistance. However, deletion of an unrelated gene, *RTA3*, results in increased miltefosine sensitivity in *C. albicans* [33]. Rta3 is a member of the Rta1/Rsb1-like family in *S. cerevisiae*, which encode putative transporters with seven transmembrane domains (TMs). ScRsb1 controls the localization of sphingoid bases in *S. cerevisiae*, including phytosphingosine and dihydrosphingosine [34, 35]. Rsb1 is localized to the membrane and is likely to act as a membrane transporter (a floppase) [7], or possibly as a regulator of transporters [36]. Overexpression of another family member, *ScRTA1*, correlates with increased resistance to 7-amino cholesterol, an inhibitor of 8-7 sterol isomerase and 14-sterol reductase [37]. The Rsb1 family members have not been fully characterised in *Candida* species. As well as showing that deleting *C. albicans RTA3* (*CaRTA3*) increases sensitivity to miltefosine, Srivastava et al [33] also showed that CaRta3 localizes to the plasma membrane, and that a fluorophore-labeled PC accumulates in the inner leaflet of the membrane in an *CaRTA3* deletion. They proposed that CaRta3 is either a floppase, or that it inhibits the activity of a flippase.

Some previous reports suggest that *CaRTA3* is also associated with resistance to azoles. Rogers and Barker [38, 39] found that transcription of *CaRTA3* is up-regulated in fluconazole-resistant isolates from AIDS patents, and Coste et al. [40] showed that Tac1p, a transcription factor regulating expression of the MDR transporters *CDR1* and *CDR2*, also regulates expression of *CaRTA3* via binding to the drug-response element. Whaley et al [41] reported that deleting *CaRTA3* reduced fluconazole resistance of a clinical isolate of *C. albicans*, and that overexpressing *CaRTA3* increased resistance. However, Srivastava et al. [33] showed that deleting *CaRTA3* in a reference isolate had no effect on fluconazole resistance. The role of Rta3 in azole resistance is therefore unclear.

In 2020, we found that the *RTA3* gene has undergone amplification in 23 clinical isolates of *Candida parapsilosis*, resulting in increased copy number of 24-33x [42]. Variable copy numbers of *RTA3* were also found by West et al [43] in four isolates. Here, by genome sequencing, we report that *RTA3* amplification is very common in *C. parapsilosis*. We find 16 distinct amplifications of *RTA3* with unique endpoints, indicative of independent and parallel amplification events. We also find a fusion to a related neighboring gene, *RTA2*. Copy number of *RTA3* is correlated with resistance to miltefosine, but not to azoles. In addition, we find that resistance to miltefosine induced by exposure to the drug is associated with loss-of-function mutations in two P4-ATPase flippase genes.

Results

C. parapsilosis phylogeny shows independent origins of *RTA3* CNVs

We explored the relationships of 170 *Candida parapsilosis* isolates using a genome-wide SNP alignment approach, generating the largest phylogeny of *C. parapsilosis* isolates to date (Fig 1). Isolates were obtained from several locations, including some previously published, and 127 that are sequenced and described here for the first time (S1 Table). Most isolates originated from the Memorial Sloan Kettering Cancer in New York (designated by MSK) and the Centre Hospitalier Universitaire de Nantes, France (designated by FM) (Fig 1).

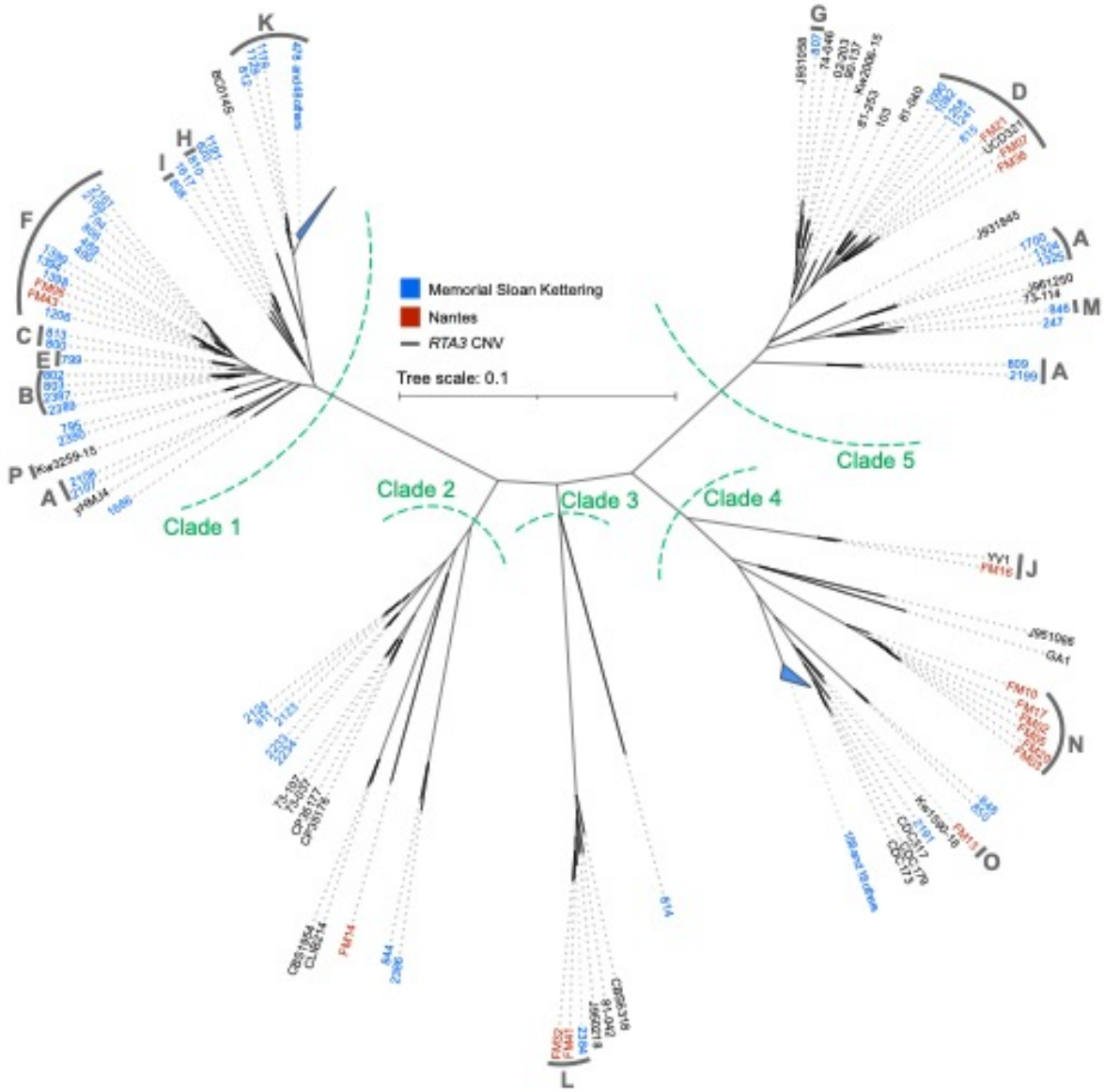

Figure 1. SNP-based unrooted phylogeny of 170 *C. parapsilosis* isolates.

Isolates harboring a CNV at *RTA3* are marked with a thick gray bar and a letter (A-P) corresponding to one of the 16 CNVs found. Isolates from Memorial Sloan Kettering Cancer Center (MSK) are named in blue (the prefix MSK is omitted from these strain names), and isolates from CHU de Nantes (FM) are named in red. Green dashed lines label each of five apparent clades. Fifty similar isolates in Clade 1, and 19 similar isolates in Clade 4, were grouped and are shown as blue triangles. The phylogeny was constructed by calling SNPs for each sample using the GATK HaplotypeCaller tool [44]. Filtered heterozygous sites were resolved using 100 iterations of Random Repeated Haplotype Sampling to provide haploid inputs for tree construction [45]. The tree was then constructed using RAxML with the GTRGAMMA model of nucleotide substitution.

148 Isolates fall into five major clades, with almost half (84/170), belonging to clade I. Most clade
149 I isolates were isolated at MSK. Half (8/16) of the FM isolates are found in Clade 4. There
150 are 49 highly similar isolates in Clade 1, and 19 highly similar isolates in Clade 4, all from
151 patients at MSK. These may have recently originated from two single isolates, and they are
152 indicated with blue triangles in Fig 1. Some other isolates (e.g. MSK2233 and MSK2234 in
153 Clade 2) may also share a recent origin. However, overall there is little evidence for
154 geographical clustering. Each clade includes at least one isolate from both MSK and FM (Fig
155 1). Three isolates from a clinical setting in Kuwait [46] are each located in a different clade
156 (designated by Kw in Fig 1). Interestingly, an environmental sample isolated from Irish soil,
157 UCD321, groups with clinical isolates from both MSK and FM (in Clade 5). The diversity of
158 isolates obtained from the same clinical setting, and the close relationship between isolates
159 from different geographical settings, highlight the global nature of *C. parapsilosis* as a
160 human pathogen.
161
162 We previously showed that the *RTA3* gene, encoding a putative floppase, had undergone
163 extensive copy number amplification in 23 *C. parapsilosis* isolates [42]. This was also
164 observed in a small number of isolates by West et al [43]. We therefore characterized copy
165 number variants (CNVs) at the *RTA3* locus in all sequenced isolates. We identified
166 increased *RTA3* copy numbers in 104 of 170 isolates. Sixteen CNVs with unique endpoints
167 were observed (assigned letters A-P, Figs. 1, 2). Nine different CNVs were observed in
168 isolates from Clade 1, whereas only CNV-L is found in isolates in Clade 3, and there are no
169 CNVs in Clade 2 isolates (Fig 1). Most (15/16) of the CNVs have a single evolutionary origin,
170 and some are present in only a single isolate (Fig 1). However, CNV-A has three separate
171 origins on the tree (one in Clade 1, and two in Clade 5).
172
173 **16 unique CNVs amplify *RTA3***
174
175 We found that *RTA3* has been amplified in 16 different types of CNV, each with unique
176 endpoints. Thirteen CNV patterns result from tandem duplications that amplify the entire
177 *RTA3* coding sequence (Fig 2A), and these repeat units range in size from 2.3 to 4.5 kb.
178 Some of these CNVs extend into the upstream neighbouring gene *MAK16,* and one (CNV-N)
179 includes the first 17 bp in the coding sequence of the downstream gene *RTA2*. The copy
180 number of *RTA3* varies both in isolates that share the same CNV, and in isolates with
181 different CNVs (Fig 2B). Isolate MSK807 (CNV-G) has the lowest estimated copy number of
182 *RTA3* among isolates with CNVs, at four copies, whereas isolate FM16 (CNV-J) has the
183 highest copy number, at 50 copies.

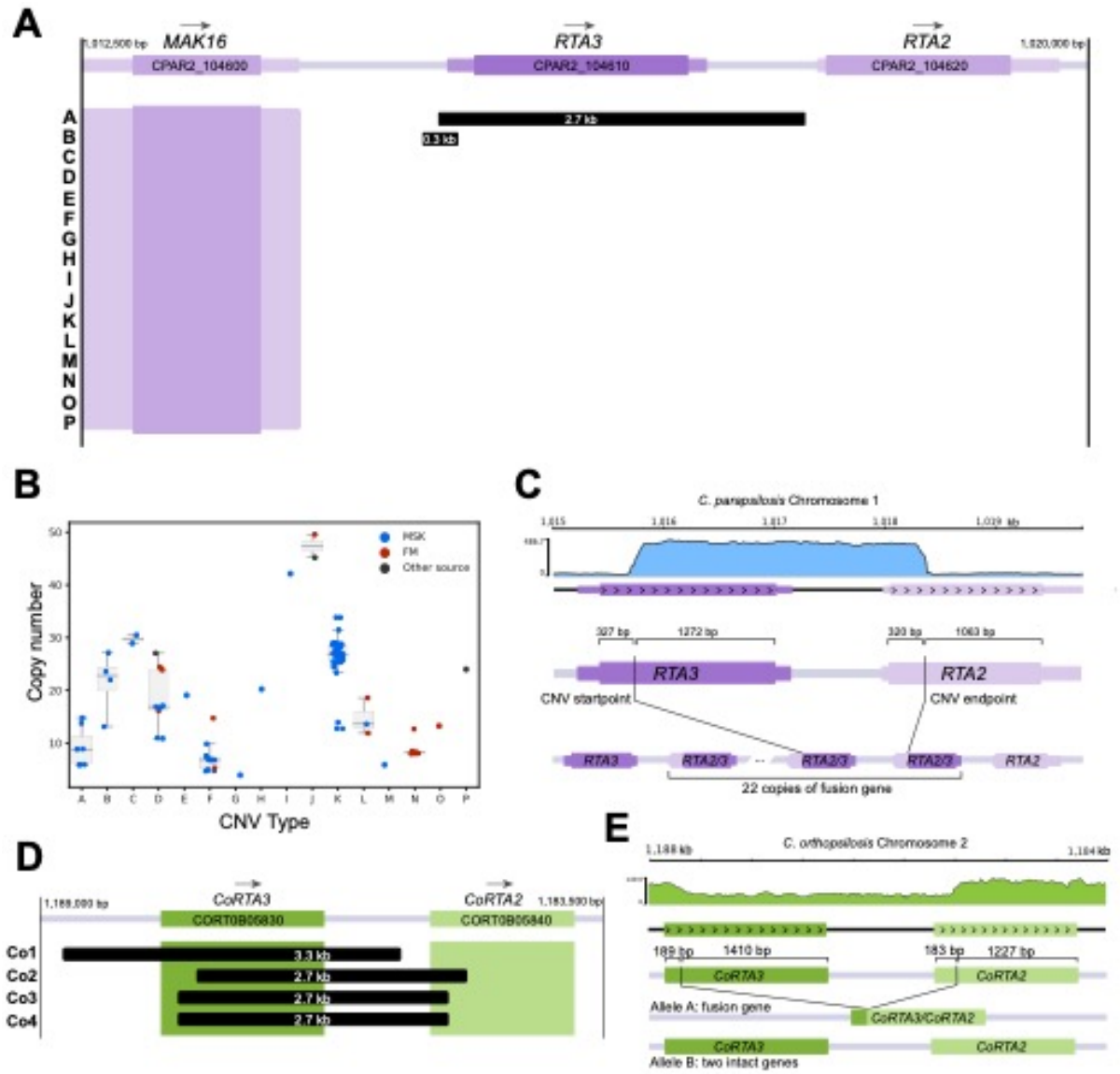

Figure 2. CNVs amplify different sequences at the *RTA3* locus

A. Span of 16 different CNVs at the *RTA3* locus in *C. parapsilosis*. The coding sequence of *RTA3* is shown by a dark purple box, with the flanking UTRs in a lighter color. The neighbouring genes *MAK16* and *RTA2* are also shown. The extents of the tandemly repeating units in each of 16 CNVs are shown by black boxes, labelled (A-P) on the left, and their lengths are indicated in white. Exact breakpoints were identified by interrogating split reads from the Illumina data, and the array structure of CNVs D and K was verified by MinION sequencing of isolates UCD321, MSK478, and MSK812.

B. Copy number of *RTA3* in each *C. parapsilosis* isolate. Each dot represents a single isolate: blue isolates from MSK, red from CHU de Nantes, and dark grey from other sources. Median and interquartile ranges are shown for CNVs present in more than one strain. Dots are jittered for clarity.

C. *RTA2/3* fusion gene in strain 434 containing CNV-P. A coverage plot created by PyGenomeTracks [47] is shown at the top. The schematic shows the position of CNV breakpoints in relation to the CDS of both genes, and the structure of the inferred array of fusion genes.

D. Amplifications of *RTA3* in *C. orthopsilosis*. Orientation of the chromosome has been flipped to highlight the similarities to *RTA3* CNVs in *C. parapsilosis*.

E. A deletion in *C. orthopsilosis* generates a *CoRTA3/CoRTA2* fusion. A coverage plot of the locus is shown at the top. The schematic shows CNV breakpoints in both *CoRTA3* and *CoRTA2* and how the resulting fusion gene is formed at one allele, leaving the other allele intact.

For CNV-K, three isolates have roughly half the *RTA3* copy number of other isolates with the same CNV (~13x instead of ~26x; Fig 2B; S1 Table). We considered the possibility that only one allele of *RTA3* was amplified in these isolates (*C. parapsilosis* is diploid), and that both alleles were amplified in other isolates. We explored this issue by using long read sequencing (Oxford Nanopore) of *C. parapsilosis* MSK812 which is one of the CNV-K isolates with fewer copies. We found that it has 8 copies of *RTA3* at one allele and 6 copies at the other (S1A Fig). Similarly, sequencing of isolate MSK478 (which also has CNV-K, with higher copy number of *RTA3*) showed that it has at least 11 copies at both alleles (S1B Fig). Therefore the variation in copy number among isolates with CNV-K is due to expansion or contraction of the array in both alleles, and not due to hemizygosity for the amplification.

Two of the *RTA3* CNVs alter the structure of the protein it encodes. The amplification in CNV-P starts within the *RTA3* open reading frame, and ends within the related adjacent gene *RTA2* (Fig 2A,C). This repeat structure generates an array of in-frame *RTA2/RTA3* gene fusions, with the N-terminus derived from *RTA2* and the C-terminus from *RTA3* (Fig 2C). *RTA3* and *RTA2* are very similar genes, which likely facilitated the fusion event. In CNV-H, the Rta3 protein is slightly truncated because this CNV consists of a tandem duplication with an endpoint 31 bp upstream of the stop codon of *RTA3*, resulting in a protein that is 10 amino acids shorter than the wild type.

CNV-B is substantially different from the others because it is an amplification of only a small region (269 bp) that is upstream and completely outside the *RTA3* coding sequence (Fig 2A). Sequencing read coverage analysis suggests that the repeat has a complex organization in which direct repeats are interspersed with inverted copies of a central segment flanked by inverted-repeats, resulting in an N:(2N-1):N copy number pattern (S2A Fig). This repeat structure was confirmed by MinION sequencing of isolates MSK802 and MSK803. The structure of the CNV-B repeat is similar to the DUP-TRP/INV-DUP structure seen in some human CNVs [48] and is reminiscent of amplifications formed via Origin-Dependent Inverted Repeat Amplification (ODIRA) [49]. The ODIRA model proposes that replication errors at origins that are surrounded by short inverted repeats generate extrachromosomal intermediates, which are then integrated at the original site [49]. This results in complex CNVs with repeat units in head-to-head and tail-to-tail arrangements that are similar to the CNV-B structure. To date, ODIRA has only been observed in *S. cerevisiae*,

237 and it is unclear whether it occurs in other yeasts [49]. If CNV-B were caused by ODIRA, we
238 would anticipate that the central region of the repeat would contain an origin of replication
239 (S2B Fig). However, determined the temporal order of replication in *C. parapsilosis* using
240 Sort-seq (S2C Fig), and we found no evidence that there is an origin near *RTA3* [50].
241
242 We also looked for evidence of *RTA3* amplification in other *Candida* species. *RTA3* is not
243 amplified in 200 sequenced *C. albicans* genomes [51, 52]. However, we identified four
244 different *RTA3* CNVs among 36 strains of *Candida orthopsilosis*, a close relative of *C.*
245 *parapsilosis* (Fig 2D). Only one of these (CNV-Co1) consists of a simple tandem
246 amplification of the entire *CoRTA3* ORF. Two others, CNV-Co2 and CNV-Co3, amplify a
247 fusion of the *CoRTA2* and *CoRTA3* genes, similar to CNV-P in *C. parapsilosis* (Fig 2D).
248 Interestingly, the final *C. orthopsilosis* CNV (CNV-Co4) involves a deletion. In the two strains
249 containing CNV-Co4, the 3' end of *CoRTA3*, the 5' end of *CoRTA2,* and the intergenic space
250 between them are deleted at one allele (Fig 2E). This results in a new fusion gene, with the
251 N-terminus derived from *CoRTA3* and the C-terminus derived from *CoRTA2*. Single copies
252 of *CoRTA2* and *CoRTA3* are intact on the other allele (Fig 2E). This is the only example we
253 have seen of an *RTA3* deletion in *C. parapsilosis, C. orthopsilosis* or *C. albicans*.
254
255 **Copy number of *RTA3* is correlated with miltefosine, but not fluconazole, resistance**

256 Deletion of *RTA3* in *C. albicans* has been shown to increase susceptibility to miltefosine [33]
257 and possibly to fluconazole [41]. We therefore investigated the effect of copy number on
258 resistance of *C. parapsilosis*. Fig 3A shows that amplification of *RTA3* is associated with
259 miltefosine resistance. For example, *C. parapsilosis* strains with only two copies of *RTA3*
260 (one at each allele, e.g. the reference strain CLIB214) fail to grow at miltefosine
261 concentrations of 10 µg/ml, whereas all the strains with *RTA3* amplifications can grow at this
262 concentration. Strains with CNVs A, H, I, J and L can tolerate miltefosine concentrations up
263 to at least 30 µg/ml, as can isolates with CNV-B (which amplifies only the region upstream of
264 *RTA3*). The CNV with the weakest effect on MF resistance is CNV-G, which can tolerate 10-
265 15 µg/ml, which is still higher than the reference strain CLIB214.

266 When different isolates carrying the same CNV are compared, miltefosine resistance is seen
267 to be correlated with the copy number of *RTA3* (Fig 3B). For example, *C. parapsilosis*
268 isolates MSK812 and MSK1129, which have 13-14 copies of CNV-K, can tolerate miltefosine
269 concentration up to ~20 µg/ml, whereas *C. parapsilosis* MSK2086 which has 27 copies
270 survives up to 30 µg/ml. Similarly, *C. parapsilosis* MSK815 with 17 copies of CNV-D and
271 MSK794 with 5 copies of CNV-F tolerate miltefosine concentrations up to ~20-25 µg/ml

272 whereas UCD321 and FM43 with 27 and 15 copies of CNV-D and CNV- F respectively
273 survive up to ~30 µg/ml (Fig 3B).

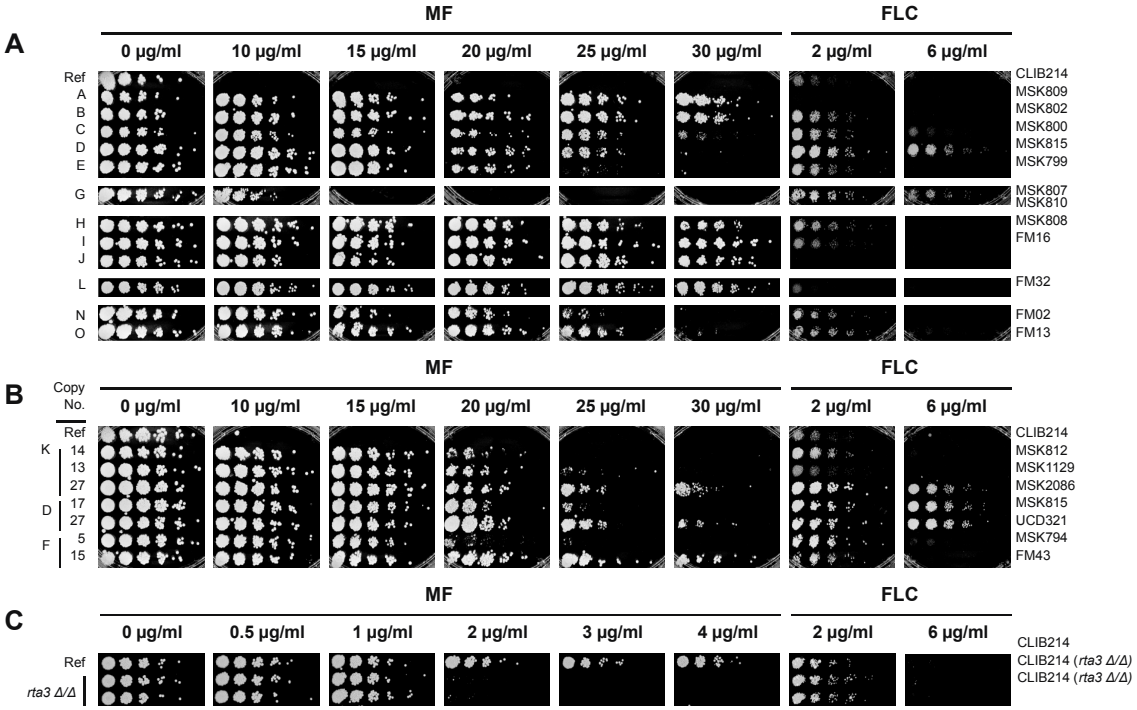

274

275 **Figure 3. CNVs of *RTA3* correlate with resistance to miltefosine**

276 A. A representative isolate of most CNV patterns (Fig 2) was grown on YPD with increasing
277 concentrations of miltefosine (MF) or fluconazole (FLC) as shown. Cells were serially diluted (1/5).
278 The CNV pattern is indicated on the left, with the strain name shown on the right. MF and FLC plates
279 were incubated for 48 hr. "Ref" indicates the reference strain *C. parapsilosis* CLIB214.

280 B. Copy number is directly correlated with miltefosine resistance. Isolates with different copy
281 numbers of CNV-K, CNV-D and CNV-F were grown as in (A). The *RTA3* copy number of each isolate
282 is shown on the left.

283 C. Deleting *RTA3* reduces resistance to miltefosine. *RTA3* was deleted in *C. parapsilosis*
284 CLIB214 using CRISPR-Cas9. The growth of two biological replicates is shown, as in (A), except that
285 incubations on FLC were for 72 h.

286

287 The isolates have variable levels of sensitivity to fluconazole (Fig 3), but the copy number of
288 *RTA3* does not correlate with susceptibility to this drug. For example, isolates MSK815 and
289 UCD321 which have 17 and 27 copies of CNV-D differ in their susceptibility to miltefosine,
290 but they both tolerate fluconazole levels of 6 µg/ml.

291 We also found that deleting *RTA3* in the reference isolate of *C. parapsilosis* (CLIB214) by
292 CRISPR-Cas9 editing [53] results in increased sensitivity to miltefosine (Fig 3C). Very low

levels of miltefosine were used (up to 4 µg/ml), because the parental strain, without any *RTA3* amplifications, is very sensitive. However, susceptibility to fluconazole was not affected by deleting *RTA3* (Fig 3C).

Increasing the *RTA3* copy number correlates with increased expression, as shown by West et al [43]. However we wondered whether amplifying the upstream region (CNV-B) has the same effect as amplifying the entire open reading frame. To explore this further, we measured *RTA3* expression by RT-PCR in one isolate of *C. parapsilosis*, MSK808, with approximately 42 copies of *RTA3* (CNV-I), and two isolates (MSK802 and MSK803) in which only the promoter region is amplified (CNV-B). We found that *RTA3* expression is approximately 22-fold higher in *C. parapsilosis* MSK808, and 2.8- to 6.6-fold higher in *C. parapsilosis* MSK802 and MSK803 than in the reference strain CLIB214 (Table 1). There are 28 copies of the direct repeat in CNV-B in *C. parapsilosis* MSK802 and 24 in *C. parapsilosis* MSK803. Thus, *RTA3* promoter region amplification (CNV-B) can lead to increased expression.

Generation of miltefosine-resistant strains by experimental evolution

The prevalence of *RTA3* amplification in *C. parapsilosis* isolates suggests that there may be some strong selective pressure inducing amplification. To determine if miltefosine is the driving force, we characterized the effect of exposing isolates to increasing concentrations of miltefosine, in an adaptive laboratory evolution approach. We started with two isolates with only one copy of *RTA3* at each allele that were in the same clade as other isolates that had undergone amplification - *C. parapsilosis* MSK795 from Clade 1, which is related to isolates that have undergone 4 different CNVs (B, C, E, and F), and *C. parapsilosis* MSK247 from Clade 5, which is related to isolates with CNVs A, D, J and M (Fig 1; Fig 4). Five lineages were evolved from MSK247 (247A to 247E) and one from MSK795 (795B). Isolates were cultured in YPD with increasing concentrations of miltefosine, up to a maximum of 32 µg/ml, over a 26-day period (Fig 4A). Sixteen randomly picked evolved colonies from each lineage tolerated miltefosine levels of 40 µg/ml (Fig 4B). The genomes of ten isolates derived from MSK247 and two from MSK795 were sequenced, together with the parental strains. The sequenced strains are listed in Methods.

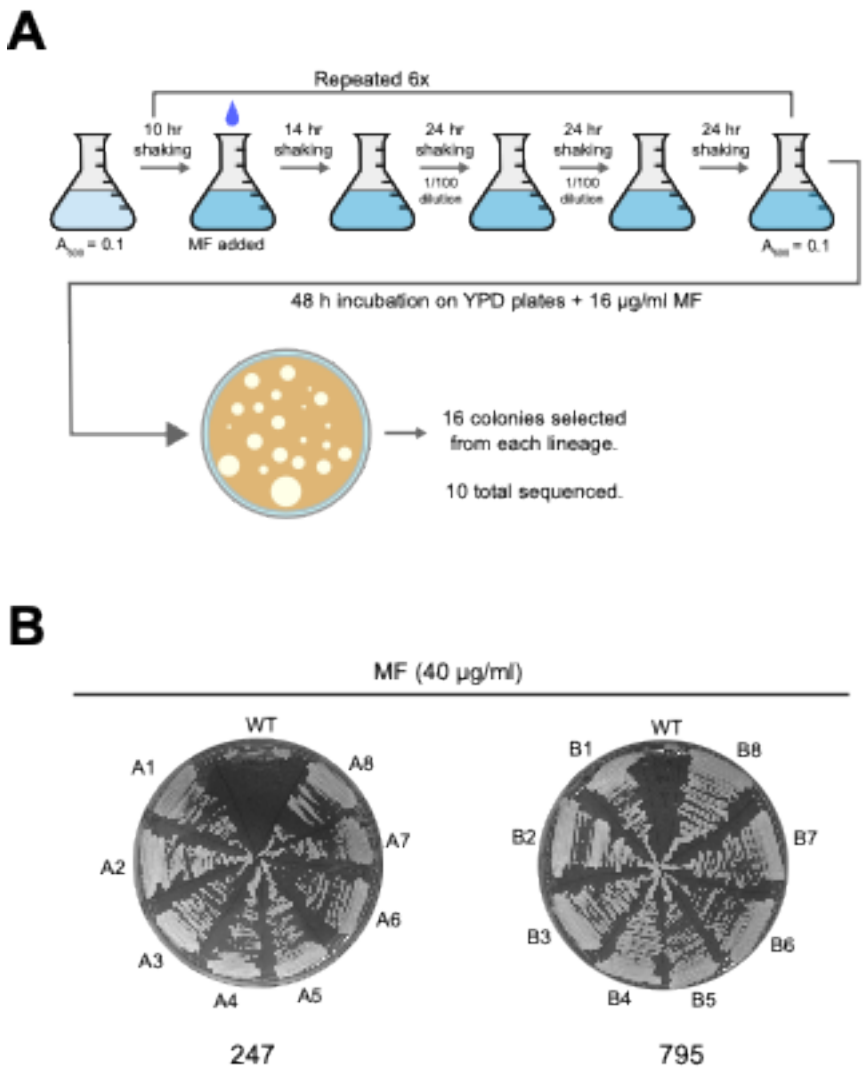

Figure 4. Generation of miltefosine-resistant *C. parapsilosis* isolates by adaptive laboratory evolution

A. Six colonies (5 derived from *C. parapsilosis* MSK247 and one from *C. parapsilosis* MSK795) were inoculated in YPD at A_{600}=0.1,and incubated at 30℃ for 10 h. Miltefosine (indicated with a blue drop) was added to a final concentration of 1 µg/ml, the cultures were incubated for a further 14 h, and then re-inoculated into the same media using a 1/100 dilution and incubated for 24 h. The dilution was repeated every 24 h for 3 days. Cells were then inoculated in fresh media, grown for 10 h, and the miltefosine concentration was doubled. The process was repeated until the concentration of miltefosine reached 32 µg/ml (24 days). On day 25, the overnight cultures were plated on YPD with 16 µg/ml miltefosine. Sixteen colonies picked from each lineage for further analysis, and the genomes of 10 were sequenced.

B. Growth of representative isolates evolved from *C. parapsilosis* MSK247 and *C. parapsilosis* MSK795 on 40 µg/ml miltefosine. WT = parental strain.

341 **Miltefosine-resistant isolates acquired homozygous disruptions in two flippase genes**

342 We did not find any evidence of amplification of the *RTA3* locus in any of the evolved
343 miltefosine-resistant strains. However, by comparing the sequences of the evolved strains to
344 those of the parental strains, we identified two genes with homozygous loss-of-function
345 variants in all 10 resistant isolates: *CPAR2_102700* and *CPAR2_303950*. These variants
346 include frameshifts, nonsense mutations, and missense mutations that are predicted to be
347 deleterious (Fig 5A). *CPAR2_102700* and *CPAR2_303950* encode putative Class 3 P4-
348 ATPases and are homologs of the PC flippase genes *DNF1* and *DNF2* in *S. cerevisiae* (Fig
349 5B).

350 The two sequenced isolates derived from *C. parapsilosis* MSK795 (795B1 and 795B16)
351 acquired mutations in both *CPAR2_102700* and *CPAR2_303950*, whereas lineages derived
352 from *C. parapsilosis* MSK247 acquired mutations only in *CPAR2_303950* (Fig 5A). However,
353 subsequent analysis revealed that *C. parapsilosis* MSK247 contains a homozygous natural
354 variant in *CPAR2_102700*, resulting in a Trp-to-Stop nonsense mutation (W1280X; Fig 5A).
355 *C. parapsilosis* MSK247 tolerates miltefosine concentrations of 5 µg/ml, whereas *C.*
356 *parapsilosis* MSK795 fails to grow (Fig 5C). Derivatives of both parents that carry
357 homozygous inactivating mutations in both *CPAR2_30395* and *CPAR2_102700* can grow up
358 to 30 µg/ml.

359

360

361

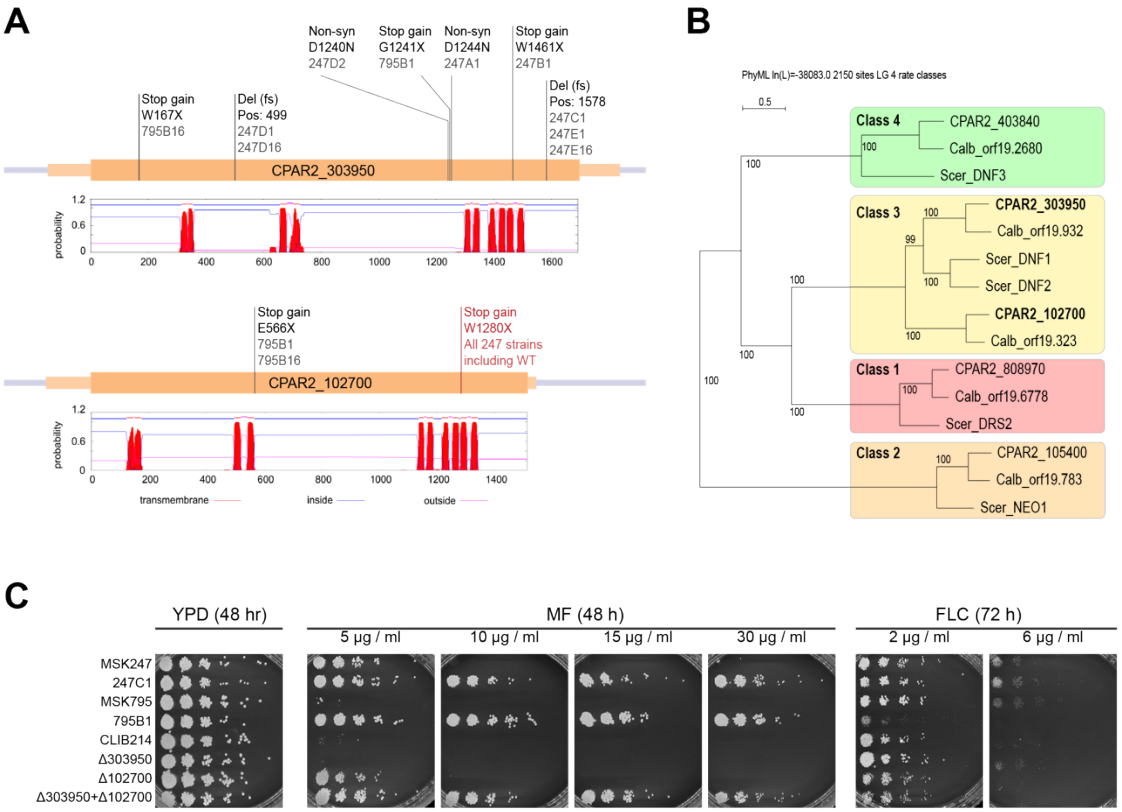

Figure 5. Protein-disrupting mutations in two flippase genes confer resistance to miltefosine in laboratory evolved strains

A. Schematic showing homozygous mutations in P4-ATPases *CPAR2_102700* and *CPAR2_303950*. Mutations named in black were acquired during the laboratory evolution experiment, in the evolved strains named below the mutation name. The mutation named in red is a natural homozygous variant found in the *C. parapsilosis* MSK247 isolate and all strains derived from it. The predicted transmembrane topology of each protein (from TMHMM [54]) is shown, where red peaks show predicted transmembrane domains.

B. Phylogeny of P4-ATPases in *C. parapsilosis*, *C. albicans*, and *S. cerevisiae*. The P4-ATPase genes in three yeast species were identified by BLAST, aligned and a tree was constructed using SeaView [55]. Monophyletic groups of genes were assigned to established classes (1-4) [56]. Both *CPAR2_102700* and *CPAR2_303950* (in bold) belong to Class 3 P4-ATPases.

C. Deleting *CPAR2_102700* and *CPAR2_303950* increases resistance to miltefosine, but not to fluconazole. *CPAR2_102700* and *CPAR2_303950* were deleted singly or together in the *C. parapsilosis* CLIB214 background, and growth was compared to isolates evolved from *C. parapsilosis* MSK247 (247C1) and *C. parapsilosis* MSK795 (795B1), as in Figure 3.

This result suggests that maximum levels of miltefosine resistance requires inactivation of both genes, *CPAR2_30395* and *CPAR2_102700*. To test this hypothesis, we deleted them, both separately and together, in the *C. parapsilosis* CLIB214 genetic background using

383 CRISPR-Cas9 editing (Fig 5C). Deleting *CPAR2_102700* alone in *C. parapsilosis* CLIB214
384 allows growth up to 5 µg/ml miltefosine, whereas deleting *CPAR2_303950* alone has no
385 effect (Fig 5C). However, strains in which both *CPAR2_303950* and *CPAR2_102700* are
386 deleted tolerate at least 30 µg/ml miltefosine, a similar concentration to strains derived from
387 the experimentally evolved isolates (MSK795B1, MSK247C1) (Fig 5C). Deleting
388 *CPAR2_102700* alone, or in combination with *CPAR2_303950*, slightly increases sensitivity
389 to fluconazole (Fig 5C).
390

391 **Discussion**

392 There is some debate over whether Rta3-like proteins are transporters or signaling
393 receptors. Rta3 is a member of the Rta1-family, which encodes proteins with 7
394 transmembrane domains, similar to the structure of G-protein-coupled receptors (GPCRs)
395 [7]. Within this family, Rta3 is more closely related to *S. cerevisiae* Rsb1 than to other
396 members. Most of the early evidence suggested that Rsb1 directly flips LCBs in the plasma
397 membrane [35]. However, Johnson et al [36] suggested that rather than acting as a
398 transporter, Rsb1 determines resistance to the LCB phytosphingosine by regulating
399 endocytosis of the tryptophan transporter Tat2, either by signalling through a G-protein (as a
400 GPCR), or by an arrestin-mediated effect on targeting of ubiquitin ligases. In addition,
401 Srivistava et al (2017) found that deleting *RTA3* in *C. albicans* resulted in increased flipping
402 of a fluorescently labelled PC, possibly by controlling activity of an unknown flippase [33].

403 However, several pieces of evidence suggest that Rsb1 is a direct lipid transporter,
404 specifically a floppase. Firstly, Rsb1 shares no sequence similarity with other yeast GPCRs
405 [7]. Secondly, Makuta et al [57] showed that Rsb1 (and not other Rta1-family members)
406 regulates LCB transport, and that this activity is dependent on a loop region following TMS5,
407 and not the C-terminus as expected for a GPCR. Rsb1 in *S. cerevisiae* and Rta3 in *C.*
408 *albicans* are located in the plasma membrane [33, 34, 41]. The increased flipping observed
409 by Srivistava et al (2017) [33] may be due to crosstalk between sphingolipids and
410 glycerophospholipids (e.g. PC), as shown in *S. cerevisiae* by Kihara and Igarashi (2004)
411 [35]. Changes in the distribution of one may be compensated by changing the distribution of
412 the other [7]. The association of *RTA3* copy number amplification with miltefosine resistance
413 in *C. parapsilosis* is also consistent with a role as a transporter. It is therefore likely that Rta3
414 is a transporter of LCBs, similar to Rsb1, and that its overexpression and deletion cause
415 changes in the localization of both PC and LCBs. Our results also suggest that *C.*
416 *parapsilosis CPAR2_102700* and *CPAR2_303950*, members of the class 3 family of P4-
417 ATPases, are the direct flippases of PC. Our data however cannot rule out the alternative

model of Johnson et al [36] whereby Rta3 regulates the function of *CPAR2_102700* and *CPAR2_303950*, rather than directly acting as a transporter.

RTA3 is adjacent to a paralogous gene (called *RTA2*) in many species in the *Candida* (CUG-Ser1) clade [58, 59]. In fact, *C. parapsilosis* CNV-P results from amplification of an *RTA3/RTA2* fusion, with the N-terminus derived from Rta2 and the C-terminus from Rta3 (Fig 2C). Deleting *RTA2* in *C. albicans* increases sensitivity to azole drugs, and overexpression increases resistance [60]. Whaley et al [41] showed that deleting *RTA3* increases sensitivity of an azole-resistant isolate of *C. albicans*, but does not have any effect on a reference isolate. Our results show that *C. parapsilosis RTA3* is unlikely to play any role in azole resistance: deleting the gene does not increase sensitivity, and levels of resistance are not associated with *RTA3* copy number in several different genetic backgrounds. However, the sequence similarity between *RTA2* and *RTA3* in *C. parapsilosis* (and in the related species *C. orthopsilosis* and *C. metapsilosis*) is much higher than between *C. albicans RTA2* and *RTA3* (S3A Fig). This similarity, and the phylogenetic relationship among these sequences (S3A Fig), indicates that in the ancestor of *C. parapsilosis*/*C. orthopsilosis*/*C. metapsilosis*, a gene conversion event occurred in which *RTA3* overwrote *RTA2*. The biggest difference between Rta3 and Rta2 in *C. parapsilosis* is that the former has a longer C-terminus (S3B Fig). Because we have never observed amplifications of *RTA2* in miltefosine-resistant *C. parapsilosis* isolates, we suggest that the two genes may have different functions, and that the difference may be related to the C terminus. In *C. albicans*, *RTA2* (and possibly *RTA3*) also contribute to tunicamycin-induced ER stress, which has not been tested in *C. parapsilosis* [61, 62].

Of the 14 CNVs resulting in tandem array amplification of *RTA3,* only CNV-A and CNV-E have obvious repeat sequences at the CNV endpoints, direct repeats of 19 bp and 10 bp respectively. The other 12 either have no repeats, or the repeat is <4 bp. The longer repeat sequence at the breakpoints of CNV-A may explain why it has originated independently three times (Fig 1). CNV-A and CNV-E may result from non-allelic homologous recombination between the direct repeats [48]. It is likely that CNV-P also originated by non-allelic homologous recombination due to the high sequence similarity between *RTA3* and *RTA2*. CNVs with shorter direct repeats at their endpoints may result from microhomology-mediated break induced replication [63]. However, there is no obvious mechanism for CNVs with no repeats at the breakpoints.

CNV-B (upstream from the coding sequence) is particularly intriguing, because it results in inversions and triplications of part of the repeated sequence (S2A Fig). This structure is

453 reminiscent of the origin-dependent ODIRA model for CNV generation [49]. We did not find
454 any evidence of a replication origin in the amplified sequence (S2A Fig), but it remains
455 possible that a rarely used origin is present. It is likely that the amplified region contains a
456 promoter because expression of *RTA3* is increased (Table 1).

457 Our results strongly suggest that there is selective pressure driving amplification of *RTA3* in
458 *C. parapsilosis*. This conclusion is based on our observation that amplification occurred in
459 isolates from diverse genetic and environmental backgrounds, distributed across the *C.*
460 *parapsilosis* phylogeny (Fig 1). We also found that there have been multiple independent
461 events of amplification, with at least 16 unique endpoints. West et al (2021) previously
462 described *RTA3* amplifications in 4 *C. parapsilosis* isolates, including one from the New York
463 subway [43]. Those amplifications also have different endpoints, but because the data
464 comes from metagenomics analyses, we cannot determine if their endpoints differ from the
465 16 CNVs we describe.

466 The CNVs sometimes encompass parts of the adjacent genes, but *RTA3* is the only
467 complete gene amplified in all of them (except for CNV-B, where its likely promoter is
468 amplified, and CNV-H where its 3' end is slightly truncated in the amplified copies). The
469 majority of the isolates in this study originated from clinical sources, although one with an
470 *RTA3* amplification (*C. parapsilosis* UCD321) has an environmental origin (it was isolated
471 from soil). There are several known examples of environmental conditions that induce or
472 selecting for CNVs, such as copper resistance resulting from amplification of *CUP1* in *S.*
473 *cerevisiae* [64, 65], and CNVs associated with growth of *C. albicans* in the presence of
474 fluconazole [66]. It is highly unlikely that the *RTA3* amplifications we discovered were driven
475 by exposure to miltefosine because it is not a commonly used antifungal drug and, as we
476 have shown, exposure to miltefosine is more likely to result in loss-of-function mutations in
477 flippase genes. At present, we do not know what kind of selective pressure led to the
478 widespread amplifications of *RTA3* in *C. parapsilosis*.
479
480 Miltefosine has potential as an antifungal drug [20-22], and it has recently been designated
481 as an orphan drug for the treatment of invasive candidiasis
482 (https://www.accessdata.fda.gov/scripts/opdlisting/oopd/detailedIndex.cfm?cfgridkey=843921). H
483 owever, our analyses suggest that it would be a poor choice, at least for invasive *Candida*
484 *parapsilosis* infections. Many isolates are naturally resistant because of amplifications of
485 *RTA3*, and in others, resistance rapidly arises due to loss-of-function mutations in the
486 flippase genes. Although mutations in two flippase genes are required for resistance, we
487 note that many of the *C. parapsilosis* samples we examined (56 of 170) have predicted loss-

488 of-function variants in *CPAR2_102700*, meaning that acquiring a mutation in
489 *CPAR2_303950* would be sufficient to render them highly resistant to miltefosine.
490

491 **Materials and methods**

492

493 **Strains and growth**. Isolates used are listed in S1 Table. Isolates were maintained on YPD
494 agar (1% Bacto Yeast Extract (212750, Sigma), 2% Bacto Peptone (211677, Sigma), 2%
495 Bacto Agar (214010, Sigma), 2% D-(+)-Glucose (G8270, Sigma)), and liquid cultures were
496 grown in 5 ml YPD broth without agar at 30ºC and 200 rpm shaking overnight. For serial
497 dilutions, 0.5 ml of the overnight cultures were harvested at 13,000 rpm at room temperature
498 for 1 min, washed twice in 0.5 ml of phosphate-buffered saline (PBS) buffer (BR0014G,
499 Thermofisher), resuspended in 0.5 ml PBS, and diluted to A_{600}= 0.0625 (approximately 6.25 x
500 10^5 cells/ml) in PBS. Five-fold serial dilutions were made in PBS and transferred with a
501 pinner to YPD agar plates containing miltefosine (M5571, Sigma Aldrich) or fluconazole
502 (F8929, Sigma Aldrich) at the indicated concentrations. Pinned plates were incubated at
503 30ºC for the indicated times and photographed using a Singer PhenoBooth.
504

505 **Gene deletions/disruptions.** The entire open reading frames of *CPAR2_104610* (*RTA3*)
506 and the flippases *CPAR2_303950* and *CPAR2_102700* were deleted using CRISPR-Cas9
507 with the pCP-tRNA system, as described in Lombardi et al [53]. All primers used for gRNA
508 and repair template synthesis are listed in S2 Table.
509

510 **Microevolution of miltefosine resistant isolates**. The microevolution method was
511 modified from Papp et al [67] and Ene et al. [68]. Three colonies from *C. parapsilosis*
512 MSK247 and *C. parapsilosis* MSK795 were originally chosen. Subsequent analysis showed
513 that 5 evolved lineages were derived from *C. parapsilosis* MSK247 (247A to E), and one
514 from *C. parapsilosis* MSK795 (795B). Colonies were incubated for 10 h in 5 ml YPD at 200
515 rpm and 30ºC. Miltefosine was added to a final concentration of 1.0 µg/ml, and the cultures
516 were incubated for a further 14 h. The cultures were diluted (1:100) into fresh media
517 containing the same concentration of miltefosine every 24 h for 3 days. Overnight cultures
518 were then diluted to an A_{600} = 0.1, incubated for 10 h, and the miltefosine concentration was
519 doubled. The 5-day cycle was repeated until a concentration of 32 µg/ml of miltefosine was
520 reached (see Fig 4A). Cultures were diluted and plated on YPD agar plates containing 16
521 µg/ml miltefosine, yielding 100-200 colonies each plate, and were incubated at 30ºC for 48
522 h. The genomes of ten resistant isolates (247A1, 247B1, 247C1, 247D1, 247D2,

523 247D16,247E1, 247E16, 797B1 and 795B16), together with the parental strains were
524 sequenced by Beijing Genomic Institute via DNBseq.
525
526 **Illumina sequencing.** Illumina sequencing of MSK isolates was carried out as described in
527 Zhai et al [42]. 45 *C. parapsilosis* isolates from Centre Hospitalier Universitaire de Nantes,
528 France were screened for resistance to miltefosine, and 16 isolates were chosen for
529 sequencing. Genomic DNA was isolated from 5 ml overnight cultures in YPD at 30℃ using
530 phenol-chloroform-isoamyl alcohol extraction. Cell pellets were resuspended in 200 µl of
531 extraction buffer (Triton X 100 2% m/v, NaCl 100mM, Tris 10mM pH 7.4, EDTA 1mM, SDS
532 1% m/v), transferred to screw cap tubes, and approximately 0.3 g of acid-washed beads and
533 200 µl of Phenol-chloroform-isoamyl alcohol (25:24:1) was added. Cells were lysed using a
534 1600 MiniG bead beater from Spex SamplePrep for 6 x 30 seconds with 30 s pauses in
535 between, and then centrifuged at 14000 rpm for 10 min at room temperature. The
536 supernatant was extracted twice more with 200 µl of TE and 200 µl of phenol-chloroform-
537 isoamyl alcohol and one 30 s agitation in the bead beater. DNA was precipitated using 80 µl
538 of ammonium acetate (7.5M) and 1 ml of 100% isopropanol, washed with 1 ml of 70%
539 ethanol and air-dried. Pellets were resuspended in 400 µl of TE with 1 µl of RNAse A (100
540 mg/ml) incubated overnight at 37℃, DNA was precipitated again, and resuspended in 150 µl
541 water. Illumina sequencing was performed by the UCD Conway Genomics Core using a
542 NextSeq 500. 1 ng of gDNA was tagmented (fragmented and tagged with adapter
543 sequences) using the Nextera kit transposome, Dual-indexed paired-end libraries were
544 prepared using Nextera XT DNA Library Prep kit. An Illumina NextSeq500 mid output 300
545 cycle sequencing kit was used to prepare and run the flowcell (HVGWJAFX2).

546 **Oxford Nanopore sequencing.** Strains were grown overnight in 50 ml YPD broth and
547 genomic DNA was extracted from approximately $4x10^9$ cells using a QIAGEN Genomic-tip
548 100/G kit (10223, QIAGEN) with minor modifications. The lyticase incubation was extended
549 to 2 h, and the proteinase K incubation was extended to overnight (~15 h). DNA libraries
550 were prepared using three different kits as per manufacturer's instructions. Libraries from *C.*
551 *parapsilosis* MSK812 and UCD321 were prepared using a Ligation Sequencing Kit (SQK-
552 LSK109, Oxford Nanopore) using 1 µg of DNA per strain. DNA was repaired using a
553 NEBNext FFPE DNA Repair Mix (M6630, New England Biolabs) and NEBNext Ultra II End
554 repair/dA-tailing Module (E75460, New England Biolabs). Adapters were ligated using
555 NEBNext Quick Ligation Module (E60560, New England Biolabs). Libraries were sequenced
556 on a MinION Mk1C device. Priming, loading and washing was carried using the EXP-
557 FLP002, and SQK-LSK109 and EXP-WSH002 Oxford Nanopore kits respectively as per
558 manufacturer's instructions. The genomes were sequenced in parallel on one flow cell; the

559 first isolate (*C. parapsilosis* MSK812) was sequenced for 24 h, and the flow cell was
560 washed, re-primed and loaded with the *C. parapsilosis* UCD321 isolate for an additional ~48
561 h. Libraries from *C. parapsilosis* MSK802 and MSK803 were prepared using a Rapid
562 Barcode Sequencing Kit (SQK-RBK004, Oxford Nanopore) using 400 ng of DNA per
563 sample. Samples were multiplexed using barcodes R04 and R05 respectively. Libraries
564 were sequenced on an original MinION device for 72 h. Priming and loading was performed
565 using the EXP-FLP002 and SQK-RBK004 kits respectively. The *C. parapsilosis* MSK478
566 library was prepared using a Rapid Sequencing Kit (SQK-RAD004, Oxford Nanopore) using
567 400 ng of DNA, and sequenced for 72 h using an original MinION device. Basecalling was
568 performed for all samples using guppy_basecaller with the following parameters: "--
569 input_path fast5 --save_path fastq -c dna_r9.4.1_450bps_fast.cfg --verbose_logs --
570 cpu_threads_per_caller 5 --num_callers 10". Guppy v.4.2.2+effbaf8 was used for samples
571 MSK812 and UCD321 and Guppy v.3.6 was used for samples MSK802 and MSK803. For
572 multiplexed samples MSK802 and MSK803, demultiplexing was performed using
573 guppy_barcoder with the following parameters: "--barcode_kits SQK-RBK004 -t 30 --
574 verbose_logs --trim_barcodes". Reads were filtered using NanoFilt with the following
575 parameters: "-l 1000 -q 7" [69].

576 **Sequence analysis**. Illumina reads were trimmed with Skewer version 0.2.2 using tags "-m
577 pe -t 4 -l 35 -q 30 -Q 30" [70]. The trimmed reads were aligned to the *C. parapsilosis*
578 reference genome using bwa mem version 0.7.12 ☐. The resulting BAM files were sorted
579 and duplicate reads were marked using GenomeAnalysisToolkit (GATK version 4.0.1.2)
580 SortSam and MarkDuplicates tools respectively [44]☐. Variants were called with GATK
581 HaplotypeCaller using the tag "--genotyping_mode DISCOVERY", combined using GATK
582 CombineGVCFs and joint-genotyped using GATK GenotypeGVCFs. Variant files were
583 filtered for read depth (<15) using and genotype quality (<40) using GATK VariantFiltration.
584 Additionally, clusters of SNPs (5 SNPs in a 100bp window) were filtered using GATK
585 VariantFiltration. A custom script was used to remove variants that were flanked on either
586 side by a long string of mono- or dinucleotide repeats, and variants that were called as
587 heterozygous but had an allele depth ratio <0.25 or >0.75
588 (https://github.com/CMOTsean/milt_variant_filtration). Additionally, for tree construction,
589 indels were excluded using GATK SelectVariants with the tag "--select-type-to-include SNP".
590 For analysis of the evolved strains, a custom script was used to filter out variants in the
591 evolved strains that were also present in the respective parent strain
592 (https://github.com/CMOTsean/milt_variant_filtration).
593

SIFT4G analysis. A SIFT prediction database was created for *C. parapsilosis* using the SIFT4G algorithm [71], and the recommended Uniref90 database as a reference for protein sequences [72]. The *C. parapsilosis* prediction database was used to annotate variants from the evolved strains with whether they are likely to be deleterious to protein function.
For each annotated gene in *C. parapsilosis*, the number of evolved strains which carried a variant predicted to be protein function-affecting by SIFT in that gene was tallied. Variants were also visualised using Integrative Genomics Viewer (IGV) to manually check results [73].

Phylogeny construction. Called SNPS were concatenated and heterozygous sites were resolved randomly to either allele by 1000 iterations of Random Repeated Haplotype Sampling [45]. SNP trees were then constructed from each of the 1000 haploid inputs, using RAxML (v8.2.12) with the GTRGAMMA model of nucleotide substitution and the random number seed "-p 12345" [74]. The tree with the highest maximum likelihood score was chosen, and the remaining 999 trees were used to generate branch support values.

Estimating copy number. For each strain with a CNV at *RTA3*, the average coverage across the *RTA3* ORF was found using BEDTools coverage (v2.29.2) [75]. This value was divided by the average genome coverage (found with BEDTools genomecov) and multiplied by two to adjust for ploidy, to calculate an estimate for the copy number of *RTA3*. For CNVs that did not cover the entire *RTA3* ORF, the average coverage of a representative section of the CNV was used instead.
MinION read sequences were used to identify the exact CNV copy number for a set of strains. The respective CNV sequences plus 1 kb flanking sequence on either side, were searched against the set of MinION reads for strains MSK478, MSK802, MSK803, MSK812, and UCD321 using BLASTN (v2.10.0) [76]. The search outputs were parsed with RECON-EBB (https://github.com/CMOTsean/recon-ebb) to estimate and visualise copy number from reads which include hits for multiple copies of the CNV sequence and both regions of flanking sequence, i.e the reads which covered the entirety of the repeat region.

Replication timing profiles. Relative replication time was determined by sort-seq as described previously [77]. Briefly, replicating (S phase) and non-replicating (G2 phase) cells were enriched from an asynchronously growing culture by FACS based on DNA content. In each sample, genomic DNA was extracted and subjected to Illumina sequencing to measure relative DNA copy number. Replication timing profiles were generated by normalizing the

629 replicating (S phase) sample read count to the nonreplicating (G2) sample read count in 1-kb
630 windows.
631
632 **Quantitative RT-PCR**. Cell harvesting and RNA extraction methods were adapted from
633 Cravener and Mitchell, 2020 [78]. Cells were inoculated from overnight cultures to an A_{600} of
634 0.2 in 25 ml of pre-warmed YPD broth and incubated at 30°C for 6 h at 200 RPM using an
635 orbital shaker. Cells were then harvested via vacuum filtration using MicroPlus-21 Sterile
636 0.45µm filters (10407713, Whatman) and stored at -80°C for at least 24 h prior to RNA
637 extraction.Cells were lysed by mechanical disruption as recommended in the QIAGEN
638 RNeasy Mini Kit (74104, QIAGEN) with some modification [78]. Cells were lysed in RLT lysis
639 buffer (QIAGEN) and Phenol:Chloroform:Isoamyl Alcohol (25:24:1)(P3803, Sigma) in a 1:1
640 ratio. Lysis was performed using a 1600 MiniG from Spex SamplePrep using 30 s lysis
641 followed by 30 s chilling on ice for a total of 6 min. RNA was extracted using a QIAGEN
642 RNeasy Mini Kit followed by two rounds of DNase digestion: one on-column using the
643 QIAGEN RNase-Free DNase Set (79254, QIAGEN); and one off-column using Invitrogen's
644 TURBO DNA-free Kit (AM1907, ThermoFisher). cDNA was synthesized from 1 µg RNA
645 using M-MLV reverse transcriptase (9PIM170, Promega) and Oligo(dT)15 primers (C110A,
646 Promega), following manufacturer's instructions. qPCR was performed in 20 µl reactions
647 using 50 ng cDNA using FastStart Universal SYBR Green Master (Rox) (4913850001,
648 Sigma) as per manufacturer's instructions on an Agilent Technologies Stratagene Mx3005p
649 machine using default "two-step" settings. All primers are listed in S2 Table. Relative
650 quantification was performed using the 2(-Delta Delta C(T)) method by comparing
651 expression to *ACT1*, and using *C. parapsilosis* CLIB214 as the calibrator strain. Calculations
652 and statistics were performed in R using the pcr package [79].

653 **Data availability**. All sequencing data is deposited at NCBI under BioProject number XXXX
654 (awaiting accession numbers).
655

656 **Acknowledgements**

657 For Open Access, the authors have applied a CC BY public copyright license to any Author
658 Accepted Manuscript version arising from this submission. This work was supported by
659 Science Foundation Ireland (grant numbers 19/FFP/6668 and 18/CRT/6214 to G.B. and
660 20/FFP-A/8795 to K.H.W), the Irish Research Council (A.R.), the Chinese Scholarship
661 Scheme (FZ), Deutsche Forschungsgemeinschaft (DFG, German Research Foundation)
662 grant RO-5328/2 (T.R.), National Institutes of Health (NIH) grants R01 AI093808 (T.M.H.),
663 R21 AI156157 (T.M.H.), the Ludwig Center for Cancer Immunotherapy (T.M.H.), the Susan
664 and Peter Solomon Divisional Genomics Program (T.M.H.), and by NIH P30 CA008748

(Cancer Center Core Grant to MSKCC). CAN acknowledges support from the Biotechnology and Biological Sciences Research Council (BBSRC), part of UK Research and Innovation, Core Capability Grant BB/CCG1720/1 and the National Capability (BBS/E/T/000PR9814). Thanks to the genomics core facility in the Conway Institute UCD for help with Illumina sequencing, to Eoin Ó Cinnéide and Letal Salzberg (UCD) for help with MinION sequencing, and to Lisa Lombardi for help with the adaptive evolution experiment.

673 Table 1. Expression of *RTA3* in strains with different amplifications

Isolate	Relative Expression	Range	P Value
MSK802 (CNV-B)	6.57	2.12 - 20.35	7.37E-03
MSK803 (CNV-B)	2.79	1.24 - 6.25	3.39E-02
MSK808 (CNV-I)	22.50	6.52 - 77.62	6.92E-05
CLIB214 (Reference)	1.00	0.19 - 5.27	N/A

674

675 **References**

676 1. Renne MF, de Kroon AI. The role of phospholipid molecular species in determining
677 the physical properties of yeast membranes. FEBS Lett. 2018;592(8):1330-45.
678 2. Sharma SC. Implications of sterol structure for membrane lipid composition, fluidity
679 and phospholipid asymmetry in *Saccharomyces cerevisiae*. FEMS Yeast Res.
680 2006;6(7):1047-51.
681 3. Grillitsch K, Tarazona P, Klug L, Wriessnegger T, Zellnig G, Leitner E, et al. Isolation
682 and characterization of the plasma membrane from the yeast *Pichia pastoris*. BBA-
683 Biomemb. 2014;1838(7):1889-97.
684 4. Devaux PF, Herrmann A, Ohlwein N, Kozlov MM. How lipid flippases can modulate
685 membrane structure. BBA-Biomemb. 2008;1778(7-8):1591-600.
686 5. Andersen JP, Vestergaard AL, Mikkelsen SA, Mogensen LS, Chalat M, Molday RS.
687 P4-ATPases as phospholipid flippases—structure, function, and enigmas. Front Physiol.
688 2016;7:275.
689 6. Daleke DL. Regulation of transbilayer plasma membrane phospholipid asymmetry. J
690 Lipid Res. 2003;44(2):233-42.
691 7. Manente M, Ghislain M. The lipid-translocating exporter family and membrane
692 phospholipid homeostasis in yeast. FEMS Yeast Res. 2009;9(5):673-87.
693 8. Heimark L, Shipkova P, Greene J, Munayyer H, Yarosh-Tomaine T, DiDomenico B,
694 et al. Mechanism of azole antifungal activity as determined by liquid chromatographic/mass
695 spectrometric monitoring of ergosterol biosynthesis. J Mass Spectrom. 2002;37(3):265-9.
696 9. Joseph-Horne T, Hollomon DW. Molecular mechanisms of azole resistance in fungi.
697 FEMS Microbiol Lett. 1997;149(2):141-9.

698 10. Van den Bossche H, Willemsens G, Cools W, Marichal P, Lauwers W. Hypothesis on
699 the molecular basis of the antifungal activity of N-substituted imidazoles and triazoles:
700 Portland Press Ltd.; 1983.
701 11. Iacano AJ, Lewis H, Hazen JE, Andro H, Smith JD, Gulshan K. Miltefosine increases
702 macrophage cholesterol release and inhibits NLRP3-inflammasome assembly and IL-1β
703 release. Sci Rep. 2019;9(1):1-12.
704 12. Kaleağasıoğlu F, Zaharieva MM, Konstantinov SM, Berger MR. Alkylphospholipids
705 are signal transduction modulators with potential for anticancer therapy. Anticancer Agents
706 Med Chem. 2019;19(1):66-91.
707 13. Benaim G, Paniz-Mondolfi AE, Sordillo EM, Martinez-Sotillo N. Disruption of
708 intracellular calcium homeostasis as a therapeutic target against *Trypanosoma cruzi*. Front
709 Cell Infect Microbiol. 2020;10:46.
710 14. Roatt BM, de Oliveira Cardoso JM, De Brito RCF, Coura-Vital W, de Oliveira Aguiar-
711 Soares RD, Reis AB. Recent advances and new strategies on leishmaniasis treatment. Appl
712 Microbiol Biotechnol. 2020:1-13.
713 15. Papadakis MA, McPhee S, Rabow M. Current medical diagnosis & treatment New
714 York, NY: McGraw-Hill Education LLC; 2018.
715 16. Dos Reis TF, Horta MAC, Colabardini AC, Fernandes CM, Silva LP, Bastos RW, et
716 al. Screening of chemical llbraries for new antifungal drugs against *Aspergillus fumigatus*
717 reveals sphingolipids are involved in the mechanism of action of miltefosine. mBIO.
718 2021;12(4):e0145821. Epub 20210810. doi: 10.1128/mBio.01458-21. PubMed PMID:
719 34372704; PubMed Central PMCID: PMCPMC8406317.
720 17. Widmer F, Wright LC, Obando D, Handke R, Ganendren R, Ellis DH, et al.
721 Hexadecylphosphocholine (miltefosine) has broad-spectrum fungicidal activity and is
722 efficacious in a mouse model of cryptococcosis. Antimicrob Agents Chemother.
723 2006;50(2):414-21.
724 18. Rossi DCP, de Castro Spadari C, Nosanchuk JD, Taborda CP, Ishida K. Miltefosine
725 is fungicidal to *Paracoccidioides* spp. yeast cells but subinhibitory concentrations induce
726 melanisation. Int J Antimicrob Agents. 2017;49(4):465-71.
727 19. Wu Y, Totten M, Memon W, Ying C, Zhang SX. In vitro antifungal susceptibility of
728 miltefosine alone and in combination with amphotericin B against emerging multidrug
729 resistant *Candida auris*. Antimicrob Agents Chemother. 2019.
730 20. Barreto TL, Rossato L, de Freitas ALD, Meis JF, Lopes LB, Colombo AL, et al.
731 Miltefosine as an alternative strategy in the treatment of the emerging fungus *Candida auris*.
732 Int J Antimicrob Agents. 2020;56(2):106049.
733 21. Wu Y, Wu M, Gao J, Ying C. Antifungal activity and mode of action of miltefosine
734 against clinical isolates of *Candida krusei*. Front Microbiol. 2020;11:854.

735 22. Vila T, Ishida K, Seabra SH, Rozental S. Miltefosine inhibits *Candida albicans* and
736 non-*albicans Candida* spp. biofilms and impairs the dispersion of infectious cells. Int J
737 Antimicrob Agents. 2016;48(5):512-20.
738 23. Jiménez-López JM, Carrasco MP, Marco C, Segovia JL. Hexadecylphosphocholine
739 disrupts cholesterol homeostasis and induces the accumulation of free cholesterol in HepG2
740 tumour cells. Biochem Pharmacol. 2006;71(8):1114-21. Epub 20060208. doi:
741 10.1016/j.bcp.2005.08.001. PubMed PMID: 16466701.
742 24. Rakotomanga M, Blanc S, Gaudin K, Chaminade P, Loiseau P. Miltefosine affects
743 lipid metabolism in *Leishmania donovani* promastigotes. Antimicrob Agents Chemother.
744 2007;51(4):1425-30.
745 25. Pinto-Martinez AK, Rodriguez-Durán J, Serrano-Martin X, Hernandez-Rodriguez V,
746 Benaim G. Mechanism of action of miltefosine on *Leishmania donovani* involves the
747 impairment of acidocalcisome function and the activation of the sphingosine-dependent
748 plasma membrane Ca2+ channel. Antimicrob Agents Chemother. 2018;62(1):e01614-17.
749 26. Cuesta-Marbán Á, Botet J, Czyz O, Cacharro LM, Gajate C, Hornillos V, et al. Drug
750 uptake, lipid rafts, and vesicle trafficking modulate resistance to an anticancer
751 lysophosphatidylcholine analogue in yeast. J Biol Chem. 2013;288(12):8405-18.
752 27. Pomorski T, Lombardi R, Riezman H, Devaux PF, van Meer G, Holthuis JC. Drs2p-
753 related P-type ATPases Dnf1p and Dnf2p are required for phospholipid translocation across
754 the yeast plasma membrane and serve a role in endocytosis. Mol Biol Cell. 2003;14(3):1240-
755 54.
756 28. Hanson PK, Malone L, Birchmore JL, Nichols JW. Lem3p is essential for the uptake
757 and potency of alkylphosphocholine drugs, edelfosine and miltefosine. J Biol Chem.
758 2003;278(38):36041-50.
759 29. Pérez-Victoria FJ, Castanys S, Gamarro F. *Leishmania donovani* resistance to
760 miltefosine involves a defective inward translocation of the drug. Antimicrob Agents
761 Chemother. 2003;47(8):2397-403.
762 30. Pérez-Victoria FJ, Sánchez-Cañete MP, Seifert K, Croft SL, Sundar S, Castanys S,
763 et al. Mechanisms of experimental resistance of *Leishmania* to miltefosine: implications for
764 clinical use. Drug Resistance Updates. 2006;9(1-2):26-39.
765 31. Seifert K, Matu S, Perez-Victoria FJ, Castanys S, Gamarro F, Croft SL.
766 Characterisation of *Leishmania donovani* promastigotes resistant to
767 hexadecylphosphocholine (miltefosine). Int J Antimicrob Agents. 2003;22(4):380-7.
768 32. Mondelaers A, Sanchez-Cañete MP, Hendrickx S, Eberhardt E, Garcia-Hernandez
769 R, Lachaud L, et al. Genomic and molecular characterization of miltefosine resistance in
770 *Leishmania infantum* strains with either natural or acquired resistance through experimental
771 selection of intracellular amastigotes. PLoS One. 2016;11(4):e0154101.

772 33. Srivastava A, Sircaik S, Husain F, Thomas E, Ror S, Rastogi S, et al. Distinct roles of
773 the 7-transmembrane receptor protein Rta3 in regulating the asymmetric distribution of
774 phosphatidylcholine across the plasma membrane and biofilm formation in *Candida*
775 *albicans*. Cell Microbiol. 2017;19(12). Epub 20171004. doi: 10.1111/cmi.12767. PubMed
776 PMID: 28745020; PubMed Central PMCID: PMCPMC5720375.
777 34. Kihara A, Igarashi Y. Identification and characterization of a *Saccharomyces*
778 *cerevisiae* gene, *RSB1*, involved in sphingoid Long-chain Base release. J Biol Chem.
779 2002;277(33):30048-54.
780 35. Kihara A, Igarashi Y. Cross talk between sphingolipids and glycerophospholipids in
781 the establishment of plasma membrane asymmetry. Mol Biol Cell. 2004;15(11):4949-59.
782 36. Johnson SS, Hanson PK, Manoharlal R, Brice SE, Cowart LA, Moye-Rowley WS.
783 Regulation of yeast nutrient permease endocytosis by ATP-binding cassette transporters
784 and a seven-transmembrane protein, RSB1. J Biol Chem. 2010;285(46):35792-802.
785 37. Soustre I, Letourneux Y, Karst F. Characterization of the *Saccharomyces cerevisiae*
786 *RTA1* gene involved in 7-aminocholesterol resistance. Curr Genet. 1996;30(2):121-5.
787 38. Rogers PD, Barker KS. Evaluation of differential gene expression in fluconazole-
788 susceptible and-resistant isolates of *Candida albicans* by cDNA microarray analysis.
789 Antimicrob Agents Chemother. 2002;46(11):3412-7.
790 39. Rogers PD, Barker KS. Genome-wide expression profile analysis reveals
791 coordinately regulated genes associated with stepwise acquisition of azole resistance in
792 *Candida albicans* clinical isolates. Antimicrob Agents Chemother. 2003;47(4):1220-7.
793 40. Coste AT, Karababa M, Ischer F, Bille J, Sanglard D. *TAC1*, transcriptional activator
794 of *CDR* genes, is a new transcription factor involved in the regulation of *Candida albicans*
795 ABC transporters *CDR1* and *CDR2*. Eukaryot Cell. 2004;3(6):1639-52.
796 41. Whaley SG, Tsao S, Weber S, Zhang Q, Barker KS, Raymond M, et al. The *RTA3*
797 gene, encoding a putative lipid translocase, influences the susceptibility of *Candida albicans*
798 to fluconazole. Antimicrob Agents Chemother. 2016;60(10):6060-6.
799 42. Zhai B, Ola M, Rolling T, Tosini NL, Joshowitz S, Littmann ER, et al. High-resolution
800 mycobiota analysis reveals dynamic intestinal translocation preceding invasive candidiasis.
801 Nat Med. 2020;26(1):59-64.
802 43. West PT, Peters SL, Olm MR, Feiqiao BY, Gause H, Lou YC, et al. Genetic and
803 behavioral adaptation of *Candida parapsilosis* to the microbiome of hospitalized infants
804 revealed by *in situ* genomics, transcriptomics, and proteomics. Microbiome. 2021;9(1):1-17.
805 44. McKenna A, Hanna M, Banks E, Sivachenko A, Cibulskis K, Kernytsky A, et al. The
806 Genome Analysis Toolkit: a MapReduce framework for analyzing next-generation DNA
807 sequencing data. Genome Res. 2010;20(9):1297-303.

808 45. Lischer HE, Excoffier L, Heckel G. Ignoring heterozygous sites biases phylogenomic
809 estimates of divergence times: implications for the evolutionary history of Microtus voles. Mol
810 Biol Evol. 2014;31(4):817-31.
811 46. Asadzadeh M, Dashti M, Ahmad S, Alfouzan W, Alameer A. Whole-Genome and
812 Targeted-Amplicon sequencing of fluconazole-susceptible and-resistant *Candida*
813 *parapsilosis* isolates from Kuwait reveals a previously undescribed N1132D polymorphism in
814 CDR1. Antimicrob Agents Chemother. 2021;65(2):e01633-20.
815 47. Lopez-Delisle L, Rabbani L, Wolff J, Bhardwaj V, Backofen R, Grüning B, et al.
816 pyGenomeTracks: reproducible plots for multivariate genomic datasets. Bioinformatics.
817 2021;37(3):422.
818 48. Carvalho CM, Zhang F, Liu P, Patel A, Sahoo T, Bacino CA, et al. Complex
819 rearrangements in patients with duplications of MECP2 can occur by fork stalling and
820 template switching. Hum Mol Genet. 2009;18(12):2188-203.
821 49. Brewer BJ, Payen C, Di Rienzi SC, Higgins MM, Ong G, Dunham MJ, et al. Origin-
822 dependent inverted-repeat amplification: tests of a model for inverted DNA amplification.
823 PLoS Genet. 2015;11(12):e1005699.
824 50. Müller CA, Hawkins M, Retkute R, Malla S, Wilson R, Blythe MJ, et al. The dynamics
825 of genome replication using deep sequencing. Nucleic Acids Res. 2014;42(1):e3-e.
826 51. Ropars J, Maufrais C, Diogo D, Marcet-Houben M, Perin A, Sertour N, et al. Gene
827 flow contributes to diversification of the major fungal pathogen *Candida albicans*. Nat
828 Commun. 2018;9(1):2253. Epub 20180608. doi: 10.1038/s41467-018-04787-4. PubMed
829 PMID: 29884848; PubMed Central PMCID: PMCPMC5993739.
830 52. Sitterlé E, Maufrais C, Sertour N, Palayret M, d'Enfert C, Bougnoux ME. Within-host
831 genomic diversity of *Candida albicans* in healthy carriers. Sci Rep. 2019;9(1):2563. Epub
832 20190222. doi: 10.1038/s41598-019-38768-4. PubMed PMID: 30796326; PubMed Central
833 PMCID: PMCPMC6385308.
834 53. Lombardi L, Oliveira-Pacheco J, Butler G. Plasmid-based CRISPR-Cas9 gene
835 editing in multiple *Candida* species. mSphere. 2019;4(2):e00125-19.
836 54. Krogh A, Larsson B, Von Heijne G, Sonnhammer EL. Predicting transmembrane
837 protein topology with a hidden Markov model: application to complete genomes. J Mol Biol.
838 2001;305(3):567-80.
839 55. Gouy M, Guindon S, Gascuel O. SeaView version 4: a multiplatform graphical user
840 interface for sequence alignment and phylogenetic tree building. Mol Biol Evol.
841 2010;27(2):221-4.
842 56. Van der Mark VA, Elferink RP, Paulusma CC. P4 ATPases: flippases in health and
843 disease. Int J Mol Sci. 2013;14(4):7897-922.

844 57. Makuta H, Obara K, Kihara A. Loop 5 region is important for the activity of the long-
845 chain base transporter Rsb1. The journal of biochemistry. 2017;161(2):207-13.
846 58. Fitzpatrick DA, O'Gaora P, Byrne KP, Butler G. Analysis of gene evolution and
847 metabolic pathways using the *Candida* Gene Order Browser. BMC Genomics. 2010;11(1):1-
848 14.
849 59. Maguire SL, ÓhÉigeartaigh SS, Byrne KP, Schröder MS, O'Gaora P, Wolfe KH, et al.
850 Comparative genome analysis and gene finding in *Candida* species using CGOB. Mol Biol
851 Evol. 2013;30(6):1281-91.
852 60. Jia X, Wang Y, Jia Y, Gao P, Xu Y, Wang L, et al. *RTA2* is involved in calcineurin-
853 mediated azole resistance and sphingoid long-chain base release in *Candida albicans*. Cell
854 Mol Life Sci. 2009;66(1):122-34.
855 61. Thomas E, Sircaik S, Roman E, Brunel J-M, Johri AK, Pla J, et al. The activity of
856 *RTA2*, a downstream effector of the calcineurin pathway, is required during tunicamycin-
857 induced ER stress response in *Candida albicans*. FEMS Yeast Res. 2015;15(8).
858 62. Yang F, Gritsenko V, Slor Futterman Y, Gao L, Zhen C, Lu H, et al. Tunicamycin
859 potentiates antifungal drug tolerance via aneuploidy in *Candida albicans*. mBIO.
860 2021;12(4):e02272-21.
861 63. Sakofsky CJ, Ayyar S, Deem AK, Chung W-H, Ira G, Malkova A. Translesion
862 polymerases drive microhomology-mediated break-induced replication leading to complex
863 chromosomal rearrangements. Mol Cell. 2015;60(6):860-72.
864 64. Fogel S, Welch JW. Tandem gene amplification mediates copper resistance in yeast.
865 Proc Natl Acad Sci (USA). 1982;79(17):5342-6.
866 65. Hull RM, Cruz C, Jack CV, Houseley J. Environmental change drives accelerated
867 adaptation through stimulated copy number variation. PLoS Biol. 2017;15(6):e2001333.
868 66. Todd RT, Selmecki A. Expandable and reversible copy number amplification drives
869 rapid adaptation to antifungal drugs. Elife. 2020;9:e58349.
870 67. Papp C, Kocsis K, Tóth R, Bodai L, Willis JR, Ksiezopolska E, et al. Echinocandin-
871 induced microevolution of *Candida parapsilosis* influences virulence and abiotic stress
872 tolerance. mSphere. 2018;3(6):e00547-18.
873 68. Ene IV, Farrer RA, Hirakawa MP, Agwamba K, Cuomo CA, Bennett RJ. Global
874 analysis of mutations driving microevolution of a heterozygous diploid fungal pathogen. Proc
875 Natl Acad Sci (USA). 2018;115(37):E8688-E97.
876 69. De Coster W, D'Hert S, Schultz DT, Cruts M, Van Broeckhoven C. NanoPack:
877 visualizing and processing long-read sequencing data. Bioinformatics. 2018;34(15):2666-9.
878 70. Jiang H, Lei R, Ding S-W, Zhu S. Skewer: a fast and accurate adapter trimmer for
879 next-generation sequencing paired-end reads. BMC Bioinformatics. 2014;15(1):1-12.

880 71. Vaser R, Adusumalli S, Leng SN, Sikic M, Ng PC. SIFT missense predictions for
881 genomes. Nat Protoc. 2016;11(1):1-9.
882 72. Suzek BE, Wang Y, Huang H, McGarvey PB, Wu CH, Consortium U. UniRef
883 clusters: a comprehensive and scalable alternative for improving sequence similarity
884 searches. Bioinformatics. 2015;31(6):926-32.
885 73. Thorvaldsdóttir H, Robinson JT, Mesirov JP. Integrative Genomics Viewer (IGV):
886 high-performance genomics data visualization and exploration. Brief Bioinform.
887 2013;14(2):178-92.
888 74. Stamatakis A. RAxML version 8: a tool for phylogenetic analysis and post-analysis of
889 large phylogenies. Bioinformatics. 2014;30(9):1312-3.
890 75. Quinlan AR, Hall IM. BEDTools: a flexible suite of utilities for comparing genomic
891 features. Bioinformatics. 2010;26(6):841-2.
892 76. Altschul SF, Madden TL, Schäffer AA, Zhang J, Zhang Z, Miller W, et al. Gapped
893 BLAST and PSI-BLAST: a new generation of protein database search programs. Nucleic
894 Acids Res. 1997;25(17):3389-402.
895 77. Batrakou DG, Müller CA, Wilson RHC, Nieduszynski CA. DNA copy-number
896 measurement of genome replication dynamics by high-throughput sequencing: the sort-seq,
897 sync-seq and MFA-seq family. Nat Protoc. 2020;15(3):1255-84. Epub 20200212. doi:
898 10.1038/s41596-019-0287-7. PubMed PMID: 32051615.
899 78. Cravener MV, Mitchell AP. *Candida albicans* culture, cell Harvesting, and total RNA
900 extraction. Bio-protocol. 2020;10(21):e3803-e.
901 79. Ahmed M, Kim DR. pcr: an R package for quality assessment, analysis and testing of
902 qPCR data. PeerJ. 2018;6:e4473.

903

904 **Supplementary Table 1** List of strains used.

905 **Supplementary Table 2**. List of primers used

906 **Supplementary Figure 1. Copy number determination of CNV-K repeat**
907 Visualisations of BLASTN results using the CNV-K repeat unit plus 1 kb flanking sequence
908 as query against MinION reads for isolates MSK478 and MSK812 where each plot
909 represents hits against a single read. Each line represents a hit, and adjacent hits are
910 separated vertically for clarity. Read identifiers are shown on the y-axis.
911 A. The exact copy number of CNV-K at both alleles was identified in isolate MSK812. (i)
912 Seven reads in the MSK812 MinION dataset have 8 copies of the CNV-K repeat unit, one is

913 shown as an example. (ii) Eighteen reads in the MSK812 dataset have 6 copies of the CNV-
914 K repeat unit, one is shown as an example.
915 B. MSK478 has at least 11 copies on both alleles. No reads in the MSK478 dataset
916 covered the entirety of the repeat array, i.e. no reads had sequence matching both sides of
917 the query flanking DNA. The read with the highest number of copies of the CNV-K repeat
918 contains 11 copies, establishing a likely lower bound for copy number at both alleles.
919
920 **Supplementary Figure 2. Structure of CNV-B**
921 A. (i) CNV-B consists of a central region (B) flanked by two regions (A and C) bounded
922 by inverted repeat pairs (inward-facing triangles). The CNV occurs upstream of the *RTA3*
923 coding sequence. (ii) CNV-B resolves as a repeat array of regions ABC interspersed with
924 inverted copies of region B.
925 B. The ODIRA model of complex CNV generation, adapted from Brewer et al (2015)
926 [49] under the terms of the Creative Commons Attribution Licence. The topmost diagram has
927 been labelled to demonstrate relationship to the observed CNV in (A).
928 C. Replication profile of strain MSK802 mapped to the *C. parapsilosis* reference
929 genome. Relative DNA copy number, as a proxy for replication time, is on the Y-axis, where
930 high values denote earlier replication. The region containing *RTA3* on chromosome 1 is
931 denoted by a red bar.
932
933 **Supplementary Figure 3. Comparison of Rta2 and Rta3 proteins.**
934 A. A phylogenetic tree was generated from Muscle alignments of Rta2 and Rta3
935 sequences from CUG-Ser species (CGOB) using PhyML, implemented in SeaView
936 [55]. Bootstrap values are shown. The pink box highlights the Rta2 and Rta3 sequences
937 from the *Candida parapsilosis* complex. The gene names are taken from the Candida Gene
938 Order Browser.
939 B. Alignment of *C. parapsilosis* Rta2 and Rta3 generated using Muscle implemented in
940 SeaView.
941